OXFORD

Cerebral Cortex, 2024, **34**, bhae186
https://doi.org/10.1093/cercor/bhae186
Advance access publication date 9 May 2024
Original Article

Aperiodic components of local field potentials reflect inherent differences between cortical and subcortical activity

Alan Bush [1,2,*], Jasmine F. Zou [3], Witold J. Lipski [4], Vasileios Kokkinos [1,2], R. Mark Richardson [1,2,3]

[1]Brain Modulation Lab, Department of Neurosurgery, Massachusetts General Hospital, Boston, MA 02114, USA
[2]Harvard Medical School, Department of Neurosurgery, Boston, MA 02115, USA
[3]Department of Brain and Cognitive Science, Massachusetts Institute of Technology, Cambridge, MA 02115, USA
[4]Department of Neurological Surgery, University of Pittsburgh, School of Medicine, Pittsburgh, PA 15213, USA
*Corresponding author: Alan Bush, Brain Modulation Lab, Department of Neurosurgery, Massachusetts General Hospital, 55 Fruit St., Thier building 429, Boston, MA 02114, USA. E-mail: Alan.bush@mgh.harvard.edu

Information flow in brain networks is reflected in local field potentials that have both periodic and aperiodic components. The $1/f^{\chi}$ aperiodic component of the power spectra tracks arousal and correlates with other physiological and pathophysiological states. Here we explored the aperiodic activity in the human thalamus and basal ganglia in relation to simultaneously recorded cortical activity. We elaborated on the parameterization of the aperiodic component implemented by *specparam* (formerly known as FOOOF) to avoid parameter unidentifiability and to obtain independent and more easily interpretable parameters. This allowed us to seamlessly fit spectra with and without an *aperiodic knee*, a parameter that captures a change in the slope of the aperiodic component. We found that the cortical aperiodic exponent χ, which reflects the decay of the aperiodic component with frequency, is correlated with Parkinson's disease symptom severity. Interestingly, no aperiodic knee was detected from the thalamus, the pallidum, or the subthalamic nucleus, which exhibited an aperiodic exponent significantly lower than in cortex. These differences were replicated in epilepsy patients undergoing intracranial monitoring that included thalamic recordings. The consistently lower aperiodic exponent and lack of an aperiodic knee from all subcortical recordings may reflect cytoarchitectonic and/or functional differences.

Significance statement
The aperiodic component of local field potentials can be modeled to produce useful and reproducible indices of neural activity. Here we refined a widely used phenomenological model for extracting aperiodic parameters (namely the exponent, offset and knee), with which we fit cortical, basal ganglia, and thalamic intracranial local field potentials, recorded from unique cohorts of movement disorders and epilepsy patients. We found that the aperiodic exponent in motor cortex is higher in Parkinson's disease patients with more severe motor symptoms, suggesting that aperiodic features may have potential as electrophysiological biomarkers for movement disorders symptoms. Remarkably, we found conspicuous differences in the aperiodic parameters of basal ganglia and thalamic signals compared to those from neocortex.

Key words: aperiodic activity; basal ganglia; thalamus; Parkinson's disease.

Introduction

From the inception of EEG, understanding the neurophysiology of oscillatory electrical activity—periodic activity of defined frequencies sustained for more than one period—has been a paramount goal (Berger 1929). These neural oscillations are widespread, spanning all brain regions and frequency bands, and correlate with many aspects of brain function and dysfunction (Engel et al. 2001; Basar and Güntekin 2013). The study of neural oscillations has also been facilitated by commonly used methods like Fourier or wavelet transforms, which can decompose any signal into a sum of oscillatory components. However, the existence and mathematical validity of these decompositions do not imply that all brain activity arises from neural oscillations. Indeed, strictly non-oscillatory processes give rise to characteristic power spectra; for example, Brownian processes are characterized by a $1/f^2$ power spectra.

Local field potentials (LFPs) reflect the ensemble activity of ionic currents of populations of cells in the vicinity of the electrode (Nunez and Srinivasan 2006; Lindén et al. 2010). The most salient feature of the frequency power spectral density (PSD) of LFPs is the decline of power with increasing frequency, a feature termed the 1-over-f ($1/f^{\chi}$, with χ denoting the aperiodic exponent) "background noise" of the spectra. Studies using LFPs commonly remove the $1/f^{\chi}$ broadband component by normalization and focus on power modulation at specific frequency bands. In contrast to the periodic nature of neural oscillations, the 1-over-f component is referred to as *aperiodic activity*.

Until recently, aperiodic activity has been largely ignored or regarded as noise, perhaps due to inadequate computational tools and theoretical framework. In pioneering work, Miller et al. fitted a parametric description of the aperiodic component to human electrocorticography (ECoG) PSD (Miller et al. 2009). The extraction of the aperiodic exponent χ has been greatly facilitated by

Received: February 24, 2023. **Revised:** April 15, 2024. **Accepted:** April 18, 2024

the development of methods like the irregular-resampling auto-spectral analysis (IRASA) (Wen and Liu 2016) and *specparam* (formerly referred to as "fitting oscillations & one-over-f" or FOOOF) (Donoghue et al. 2020). The latter fits the periodic component of the spectrum as a superposition of Gaussians and parameterizes the aperiodic component as $P_{aperiodic} = A/(k + f^{\chi})$, with an offset **A**, an aperiodic exponent $\boldsymbol{\chi}$, and an optional knee parameter **k** (Donoghue et al. 2020) (see also Supplementary Materials). Note that this method requires an a priori decision of whether to use the knee parameter or not.

Using these methods, a recent body of work explored correlations of aperiodic parameters with different behavioral, physiological, and pathophysiological states and anatomical regions. The cortical aperiodic exponent $\boldsymbol{\chi}$ decreases with age (Voytek et al. 2015; Dave et al. 2018), increases under anesthesia and during sleep (Muthukumaraswamy and Liley 2018; Colombo et al. 2019; Miskovic et al. 2019; Lendner et al. 2020), and differs across cortical regions (Muthukumaraswamy and Liley 2018; Chaoul and Siegel 2021). Likewise, the knee **k** of the spectra (i.e. the frequency at which the rate of decline of power with increasing frequency changes) also has a spatial structure in the cortex (Gao et al. 2020). Thus, aperiodic parameters are potentially useful descriptors of population-averaged neural activity recorded by LFPs.

Given the importance of understanding the cortical-subcortical neural dynamics that underlie normal human behavior and symptoms of brain diseases, we explored differences in the parameters of the aperiodic component of LFPs recorded from unique cohorts of neurosurgical patients. We elaborated on the parameterization of the aperiodic component developed by (Donoghue et al. 2020) to formulate a model with better-defined aperiodic parameters that avoids a priori assumptions on the presence of an aperiodic knee. We used this model to explore (across patients) the relation of cortical aperiodic activity with movement disorder pathophysiology and cortical anatomy in movement disorders patients undergoing deep brain stimulation (DBS) surgery. We then performed within-subject comparisons of aperiodic parameters in thalamic and basal ganglia nuclei to those in the cortex, including a second cohort of patients with drug-resistant epilepsy undergoing intracranial monitoring.

Methods

Participants

Movement disorder patients undergoing intracranial electrode implantation for DBS therapy participated in a speech production task (see task details in Bush et al. 2022 and Vissani et al. 2023), of which the baseline periods were analyzed in this study. Briefly, the speech task involved repetition of triplets of consonant-vowel syllables presented auditorily via earphones, with no visual cue, no fixation point and no working memory demand. The intervals between trials, from speech offset of a trial to cue onset of the next trial, were analyzed for each run of the task (3.0 ± 1.4 runs per participant, 118.0 ± 1.5 baseline intervals per run, 2.27 ± 0.45 s per interval, for a total baseline duration of 4.2 ± 1.1 min per run; median ± median-absolute-deviation reported in all cases). One or two high-density subdural ECoG strips were temporarily placed through the standard burr hole, targeting the left superior temporal gyrus (also covering the ventral sensorimotor cortex) and left inferior frontal gyrus. ECoG electrodes were removed at the end of the surgery. Dopaminergic medication was withdrawn the night before surgery. All procedures were approved by the University of Pittsburgh Institutional Review Board (IRB Protocol #PRO13110420), and all patients provided informed consent to participate in the study. The following cohorts of movement disorder patients participated in the study:

- 29 Parkinson's disease patients (21M/8F, 65.6 ± 7.1 years) undergoing awake subthalamic (STN) DBS surgery, 26 of which had usable ECoG recordings and 13 of which had simultaneous ECoG and DBS lead recordings (two ECoG recordings were excluded for excessive package drops and one for incomplete metadata).
- 5 Parkinson's disease patients (5M/0F, 69.1 ± 5.7 years) undergoing awake pallidal (GPi) DBS surgery, of which 4 had usable ECoG recordings, and 3 had simultaneous ECoG and DBS lead recordings (intraoperative recordings could not be completed for one subject). Given that our multidisciplinary team recommends either STN or GPi targeting based on a sum of factors such as motor symptoms and cognitive profiles, baseline neurophysiological states could be different between these two groups; thus, we segregated PD patients by the subcortical target for ECoG analysis.
- 22 essential tremor patients (11M/11F, 65.3 ± 9.7 years) undergoing awake thalamic (Vim) DBS surgery, of which 18 had usable ECoG recordings, and 15 had simultaneous ECoG and DBS lead recordings (intraoperative recordings could not be completed in two cases and data for two subjects showed strong atypical line noise).

All PD patients underwent standard preoperative evaluations, including the Unified Parkinson's Disease Rating Scale (UPDRS, (Goetz et al. 2008)) in the OFF and ON medication states (operationalized as approximately 12 h after the last dose for OFF and 1 h after administration of dopaminergic medications for ON), within 4 months prior to surgery. Subscores of UPDRS-III were defined as axial (items 1, 12–14), tremor (items 16 and 17), rigidity (item 3), and bradykinesia (items 4–6, 8 and 9). Note that there are more males than females in PD cohorts reflecting the gender gap in DBS referral and utilization (Willis et al. 2014; Jost et al. 2022).

Additionally, we analyzed intervals of awake restfulness data from 8 epilepsy patients (5M/3F, age: 18 ± 11 years) undergoing stereo-EEG (sEEG) intracranial monitoring for epilepsy with additional electrodes implanted in the thalamus (10.0 ± 4.6 min per interval, median ± MAD). Implantation of the thalamus during sEEG monitoring for patients who may be candidates for thalamic responsive neuromodulation (RNS) is considered standard-of-care at our center (Richardson 2022). This study was approved by the Massachusetts General Hospital (Boston, MA) Institutional Review Board (IRB Protocol #2020P000281).

Neural recordings

Figure 1 and Table S1 describe the electrodes used in this study. ECoG electrodes and DBS lead signals were simultaneously acquired at 30 and at 1 kHz (ns2 files bandpass filtered from 1 to 250 Hz, fourth-order Butterworth) with a Grapevine Neural Interface Processor equipped with Micro2 Front Ends (Ripple LLC, Salt Lake City, UT, USA). For computational efficiency we used the 1 kHz (ns2) recordings for analysis. ECoG and DBS lead recordings were referenced to a subdermal scalp needle electrode positioned approximately on Cz. The sEEG signals were recorded at 1-kHz sampling rate using a 128-channel Xltek digital video-EEG system (Natus Medical Incorporated, Pleasanton, CA). sEEG recordings were referenced to an EEG electrode placed extracranially (C2 vertebra or Cz).

Electrode localization

DBS electrodes were localized using the Lead-DBS localization pipeline (Horn et al. 2019). Briefly, a preoperative anatomical T1

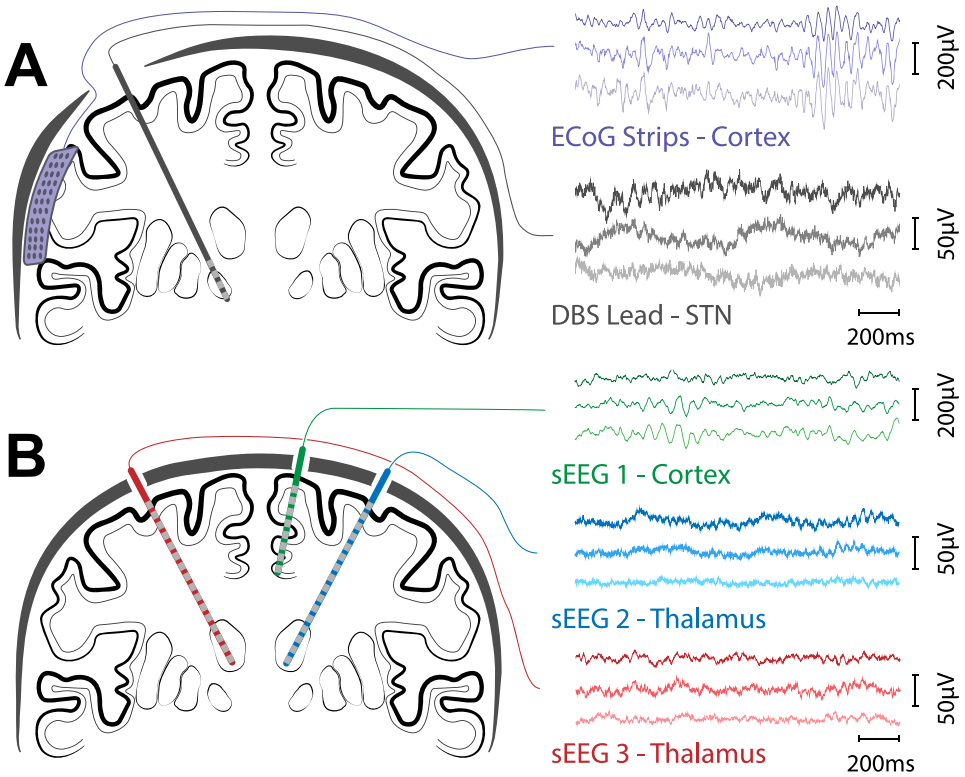

Fig. 1. Schematic representation of electrode montages. (A) Movement disorder patients undergoing DBS implantation surgery with simultaneous multichannel recordings from DBS leads and ECoG strips implanted in the left hemisphere. (B) Epilepsy patients undergoing intracranial monitoring with multichannel sEEG electrodes, some targeting thalamic nuclei. Schematic representation of a coronal sections (neurological convention) on the left, and examples of raw voltage traces for cortical and subcortical regions on the right (DBS: deep brain stimulation, ECoG: electrocorticography, STN: subthalamic nucleus, sEEG: stereotactic electroencephalography).

weighted MRI scan was co-registered with a post-operative CT scan. The position of individual contacts was manually identified based on the CT artifact and constrained by the geometry of the DBS lead used. This process rendered the coordinates for the leads in each subject's native space. The position of the ECoG strips was calculated from intra-operative fluoroscopy as described in (Randazzo et al. 2016). Briefly, the cortical surface was reconstructed from the preoperative MRI using FreeSurfer (Fischl et al. 2002) and a model of the skull and stereotactic frame was reconstructed from the intra-operative CT scan using OsiriX (osirix-viewer.com). The position of the frame's tips on the skull and the implanted DBS leads were used as fiducial markers. The models of the pial surface, skull and fiducial markers were co-registered, manually rotated, and scaled to align with the projection observed in the fluoroscopy. Once aligned, the position of the electrodes in the ECoG strip was manually marked on the fluoroscopy image, and the projection of those positions to the convex hull of the cortical surface was defined as the electrode location in native space. The coordinates were then regularized based on the layout of the contacts in the ECoG strip (github.com/Brain-Modulation-Lab/ECoG_localization). All coordinates were then transformed to the ICBM MNI152 Non-Linear Asymmetric 2009b space (Fonov et al. 2011) using the Symmetric Diffeomorphism algorithm implemented in the Advanced Normalization Tools (Avants et al. 2008).

Epilepsy patients were implanted with commercially available 8–16 contact electrodes (PMT Corporation, MN, USA; AdTech Medical Instrument Corporation, WI, USA). Electrode trajectories were tailored for each patient according to the surgical hypothesis, and contact locations were determined by either post-implantation MRI or co-registration of the preoperative T1 MRI with the post-implantation CT using Brainstorm (Tadel et al. 2011).

Anatomical labels were assigned to each electrode based on the HCP-MMP1 atlas (Glasser et al. 2016) for cortical electrodes and the Morel (Morel 2007) and DISTAL (Ewert et al. 2018) atlases for subcortical electrodes.

Electrophysiological data preprocessing and power spectrum estimation

Data recorded during DBS surgeries were processed using custom code based on the FieldTrip (Oostenveld et al. 2011) toolbox implemented in MATLAB, available at (github.com/Brain-Modulation-Lab/bml). Data were loaded from 1-kHz ns2 files, low pass filtered at 250 Hz using a fourth-order Butterworth filter and stored as continuous recordings in FieldTrip datatype-raw. No notch filter was applied. Electrodes were common average referenced per head-stage connector and electrode type. sEEG data recorded for epilepsy monitoring was loaded from 1 kHz EDF files, bandpass filtered from 1 to 250 Hz with a fourth-order Butterworth filter and common-average referenced for consistency with DBS data. For all data, PSD was estimated using the Welch method (Welch 1967), using 1-s time windows with a 50% overlap.

Spectral parameterization

We elaborated upon the spectral parameterization introduced by Donoghue et al. (2020) to capture the frequency domain characteristics of electrophysiological data. This parameterization decomposes the log-power spectra $\mathbf{log}\,(\mathbf{P}\,(f))$ into an aperiodic component $\mathbf{log}\,(\mathbf{L}\,(f))$ and the summation of $\mathbf{N}$ narrow-band

periodic components that are each modeled as a Gaussian:

$$\log\left(P\left(f\right)\right) = \log\left(L\left(f\right)\right) + \sum_{n=0}^{N} a_n\, e^{-\frac{(f-fc,n)^2}{2w_n{}^2}} \quad (1)$$

where f is the frequency, a_n is the power, $f_{c,n}$ the center frequency, and w_n is the width of the Gaussian n (i.e. the standard deviation). Gaussians were used to model physiological oscillations and spectral artifacts like line noise. This approach was preferred over notch filters as the model does not adequately fit spectra with notches. In this work, we propose a new parameterization of the aperiodic component defined as

$$L\left(f\right) = A\frac{f_k{}^{\chi} + f_{min}^{\chi}}{f_k{}^{\chi} + f^{\chi}} \quad (2)$$

where A is the aperiodic offset and can be interpreted as the power fitted at the minimal frequency of interest f_{min}, defined as the smallest positive frequency for which power can be reliably estimated based on acquisition, preprocessing, and PSD estimation methods. For the current work, it was defined as $f_{min} = \max\{f_{HP}, f_s/m\}$, the largest between f_{HP}, the cutoff frequency of the high-pass filter applied at acquisition (or preprocessing), and the smallest positive frequency calculated by the Welch method f_s/m, where f_s is the sampling rate and m the number of samples in the Welch window. The parameter f_k is the knee frequency at which there is a change in log–log slope of the PSD and, for $f_k \gg f_{min}$, corresponds to the frequency at which the power decays to A/2. The rate at which the power decreases for frequencies above f_k is defined by the aperiodic exponent χ. We also modified the original algorithm proposed by Donoghue et al. (2020) to scan f_k logarithmically (defining the auxiliary parameter $pf_k = \log_{10}(f_k)$, substituting $f_k \rightarrow 10^{pf_k}$ in Equation (2), and optimizing over pf_k), therefore ensuring positive values for f_k. This change also allows the full model to adequately fit cases with no knee in the PSD by converging to $f_k < f_{min}$. For computational reasons, we restricted the range of f_k from $f_{min}/10$ to f_{LP}. See the supplementary materials for a discussion on the advantages of using this parameterization over the original one proposed by Donoghue et al. (2020). Note that the model was fitted to PSDs from individual channels and runs, and the extracted aperiodic parameters were then aggregated for statistical analyses. The *aperiodic neural timescale* τ can be calculated from the aperiodic knee as $\tau = (2\pi f_k)^{-1}$, as defined in Gao et al. (2020). Other parameters for *specparam* were not modified relative to the original model (v1.1.0) and were kept constant at peak_width_limits = [2,25], max_n_peaks = 6, min_peak_height = 0.15, peak_threshold = 2, and freq_range = [1, 250]. Additionally, we modified the cost function (J) of the fitting procedure by adding to the mean squared error term a regularization term that penalizes the integral of the Gaussians over negative frequencies (Equation 3):

$$J = \frac{1}{M}\sum_{i=1}^{M}\left(Y_i - \hat{Y}_i\right)^2 + \lambda\sum_{n=0}^{N}\int_{-\infty}^{f_{min}} G_n\left(F\right)\, dF \quad (3)$$

where Y_i is the log power estimated by the Welch method at frequency f_i, and $\hat{Y}_i$ is the value fitted by the model. The second term was added to prevent Gaussian peaks from extending beyond the fitting range, which can affect the estimation of the aperiodic component (Gerster et al. 2022). The regularization parameter λ was empirically adjusted for each dataset. Algorithm development and analyses for this work were done in Python. The modified *specparam* package is available at github.com/Brain-Modulation-Lab/fooof/tree/lorentzian.

Statistical analysis

We performed statistical analyses in R. Base functions were used for correlation tests, paired Wilcoxon tests, linear models, and Fisher exact test for count data. The *coin* package was used for the approximative K-Sample Fisher–Pitman permutation tests (Hothorn et al. 2008), in which cohort labels or anatomical locations were permuted across subjects 9,999 times. The *lmerTest* package was used for linear mixed effects models (Kuznetsova et al. 2017) and *multcomp* for multiple comparisons (Bretz et al. 2011). Analysis scripts and tabulated data is available at github.com/Brain-Modulation-Lab/Paper_AperiodicComponent.

Results

To explore differences between the aperiodic components of cortical and basal ganglia or thalamic LFPs, we elaborated upon the *specparam* method (Donoghue et al. 2020) by incorporating a new Lorentzian-like parameterization of the aperiodic component, changing the way parameters are scanned and adding a regularization term (see methods and supplementary materials for details). These changes result in more easily interpretable parameters, with well-defined units and better parameter identifiability (Cedersund and Roll 2009) (Fig. S1). In our new parameterization of the aperiodic component (Equation 2), the offset A represents the power density at the smallest positive frequency acquired f_{min}, the aperiodic exponent χ is the rate of decline of power with frequency, and the knee f_k is the frequency at which there is a change in the rate of decline (Fig. 2A). These modifications also allow the fitting of the same model to power spectra with qualitatively different profiles. In the original description, parameterization required an a priori selection of one of two possible models (with or without a "knee" parameter); our modifications allow seamless fitting of either case with the same model, without compromising the interpretability of the parameters (Fig. S2).

First, to assess the performance of the novel parameterization, we fitted the power spectra of ECoG recordings acquired from movement disorder patients undergoing awake DBS implantation surgery. Baseline epochs recorded during rest periods in a speech production task were used for this analysis. The novel parameterization fits the data as well as the original implementation (Fig. 2A); R^2 values of both models are virtually identical and tightly cluster at values above 0.975 (Fig. 2A inset). Furthermore, the aperiodic parameters for the novel formulation do not show the strong collinearity observed for the parameters of the original model (Figs 2B, S3A, and S3B) which indicates poor parameter identifiability in the original model, leading to larger uncertainties in the parameter values (Cedersund and Roll 2009). Note, however, that there is a residual correlation between the aperiodic knee and the exponent of cortical spectra (Fig. S3B) and for STN spectra both parameterizations show similar correlation between exponent and offset (Fig. S3C). Our novel formulation also better constrains the range of values of the parameters; for example, the aperiodic offset spans six orders of magnitudes for the original model but only two in the novel formulation (Fig. 2B).

We explored cortical aperiodic activity from ECoG recordings in PD patients undergoing STN-DBS implantation using our new parameterization. Across participants, electrodes (blue dots in Fig. 3A) covered the left dorsolateral-prefrontal, inferior-frontal,

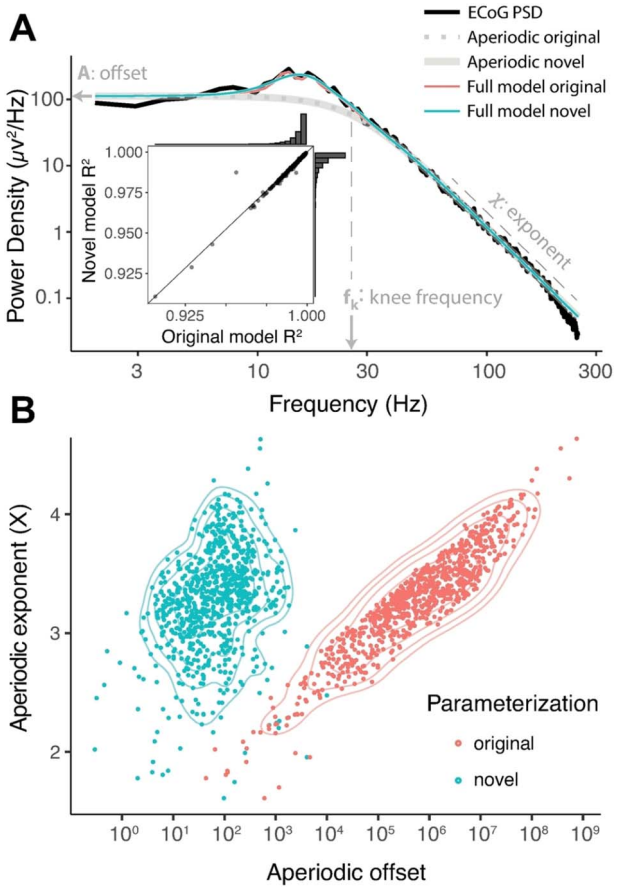

Fig. 2. The novel parameterization of the aperiodic component avoids collinearity between parameters. (A) Representative example of cortical power spectra with fits from original and novel models (as indicated in the legend). Novel aperiodic parameters are represented on the plot: A is the power density at the smallest frequency acquired, χ is the negative log–log slope, and f_k is the frequency at which the slope changes. The inset shows the correlation between R^2 values for both models, and their univariate distribution in data from PD participants. (B) Aperiodic exponent vs. offset parameters for ECoG recordings from a random subset of 11 PD patients undergoing STN (9) or GPi (2) DBS, for the original and novel parameterizations. Each point represents parameters from an electrode. Contour lines represent the 5, 10, 20, 40, and 80% percentiles of 2D kernel density estimation (ECoG: electrocorticography, PSD: power spectral density).

premotor, sensorimotor, posterior-opercular, inferior-parietal, temporo-parietal-occipital, and auditory-associative cortex (regions defined by the MMP1 atlas (Glasser et al. 2016), Fig. 3B central panel, see Fig. S4A for group-level PSDs from all regions sampled). Interestingly, we found a significant positive correlation between the preoperative UPDRS-III ON score (a clinical measure of PD motor symptom severity), and the aperiodic exponent from inferior-frontal ($\rho = 0.82$, $P = 0.016$) and dorsolateral-prefrontal cortical areas ($\rho = 0.71$, $P = 0.017$, FDR-corrected Spearman's correlation test, Fig. 3B). A post-hoc analysis in these two regions shows that the bradykinetic subscore of UPDRS-III drives the correlation with the aperiodic exponent (Fig. 3C). However, no significant correlation was found with the UPDRS-III OFF score (Fig. S5). Neither the aperiodic offset nor the aperiodic knee showed significant correlations with UPDRS-III scores in any cortical region (Spearman correlation, FDR-corrected $\alpha = 0.05$).

There was no significant difference between PD patients undergoing STN-DBS ($PD_{STN\text{-}DBS}$) and essential tremor patients undergoing VIM-DBS ($ET_{VIM\text{-}DBS}$) for the cortical aperiodic exponent ($P = 0.096$, Fisher–Pitman permutation test) or knee frequency ($P = 0.83$). However, both of these cohorts differed from $PD_{GPi\text{-}DBS}$ patients in cortical aperiodic exponent ($P = 0.031$) and aperiodic knee ($P = 0.018$, Fig. 3D). There was no difference in aperiodic offset across the three cohorts ($P = 0.51$, Fig. 3D, bottom). Due to the lack of significant difference between cortical aperiodic parameters, we pooled data across the $PD_{STN\text{-}DBS}$ and $ET_{VIM\text{-}DBS}$ cohorts for subsequent cortical analyses.

There was no significant correlation of the aperiodic exponent with age ($P = 0.23$, Spearman correlation). Note that the age range of this cohort (43–79 years) does not include the younger adult group (18–30 years) from previous studies (Voytek et al. 2015; Dave et al. 2018). We grouped electrodes according to the multimodal-parcellation atlas (HCP-MMP1; Glasser et al. 2016, Fig. 3B, center) and used a mixed-effects model to account for subject-to-subject variability. In line with recent reports (Muthukumaraswamy and Liley 2018; Gao et al. 2020; Chaoul and Siegel 2021), we found significant differences in aperiodic parameters across cortical regions (Fig. 3E, Table S2). We observed that the aperiodic knee frequency in primary sensory cortex "1" was significantly greater than that observed in premotor region "6r", posterior-opercula area 4 "OP4", and auditory-associative area "A5" (Tukey's HSD for region effect $\alpha = 0.05$). Similarly, the aperiodic exponent differed between posterior-opercular area "OP4" and sensorimotor/premotor areas "1," "3b," "55b," and "6v," and between auditory-associative area "A4" premotor areas "55b" and "6v" (Tukey's HSD for region effect $\alpha = 0.05$).

Next, we explored the aperiodic component from subcortical recordings acquired through the DBS leads. For PD patients, DBS leads targeted the dorsal-posterior-lateral portion of the subthalamic nucleus (STN) or the inferior-posterior-lateral globus pallidus internus (GPi), whereas for ET patients, leads targeted the ventral intermedius (VIM) nucleus of the thalamus (Fig. 4A). In contrast to what was observed for cortical recordings, no obvious "knee" was apparent in power spectra from the STN, VIM, or GPi (Figs 4B–D and S4B); the aperiodic component of extracellular potentials for these subcortical structures decreases with frequency starting from the minimal frequency acquired. These qualitative differences with ECoG PSDs could be due to the different electrode types (see Table S1 for details), reflect underlying electrophysiology, or a combination of both effects (see Discussion). To quantify these differences, we fit subcortical power spectra using the same model as for cortical data (Fig. 4B–D).

The distribution of aperiodic parameters in STN recordings differs remarkably from that in cortical ECoG signals from the same subjects (Fig. 4E–G, left panels). The aperiodic exponent for the STN has a median of 1.30 ± 0.21 (median ± standard deviation across subjects), almost 3-fold smaller than that of ECoG recordings 3.41 ± 0.30 for the same subjects ($P = 0.0002$, paired Wilcoxon test, Table 1, Fig. 4E). Contrary to what we observed for cortical recordings, there was no correlation between the aperiodic exponent from the STN and preoperative UPDRS-III ON or OFF scores ($P = 0.9$ and 0.6, respectively, Spearman correlation). As was the case for cortical spectra, the STN aperiodic offset does not correlate with preop UPDRS (ON or OFF). The aperiodic exponent from DBS lead recordings in VIM was also significantly different from the simultaneous cortical recordings ($P < 10^{-4}$ paired Wilcoxon test, Fig. 4E). Interestingly, the difference between cortical and subcortical aperiodic exponents reached significance for all individual subjects analyzed (Fig. 4E, FDR-corrected Fisher–Pitman permutation test), including GPi recordings for which no group-level difference was detected ($P = 0.25$, paired Wilcoxon test).

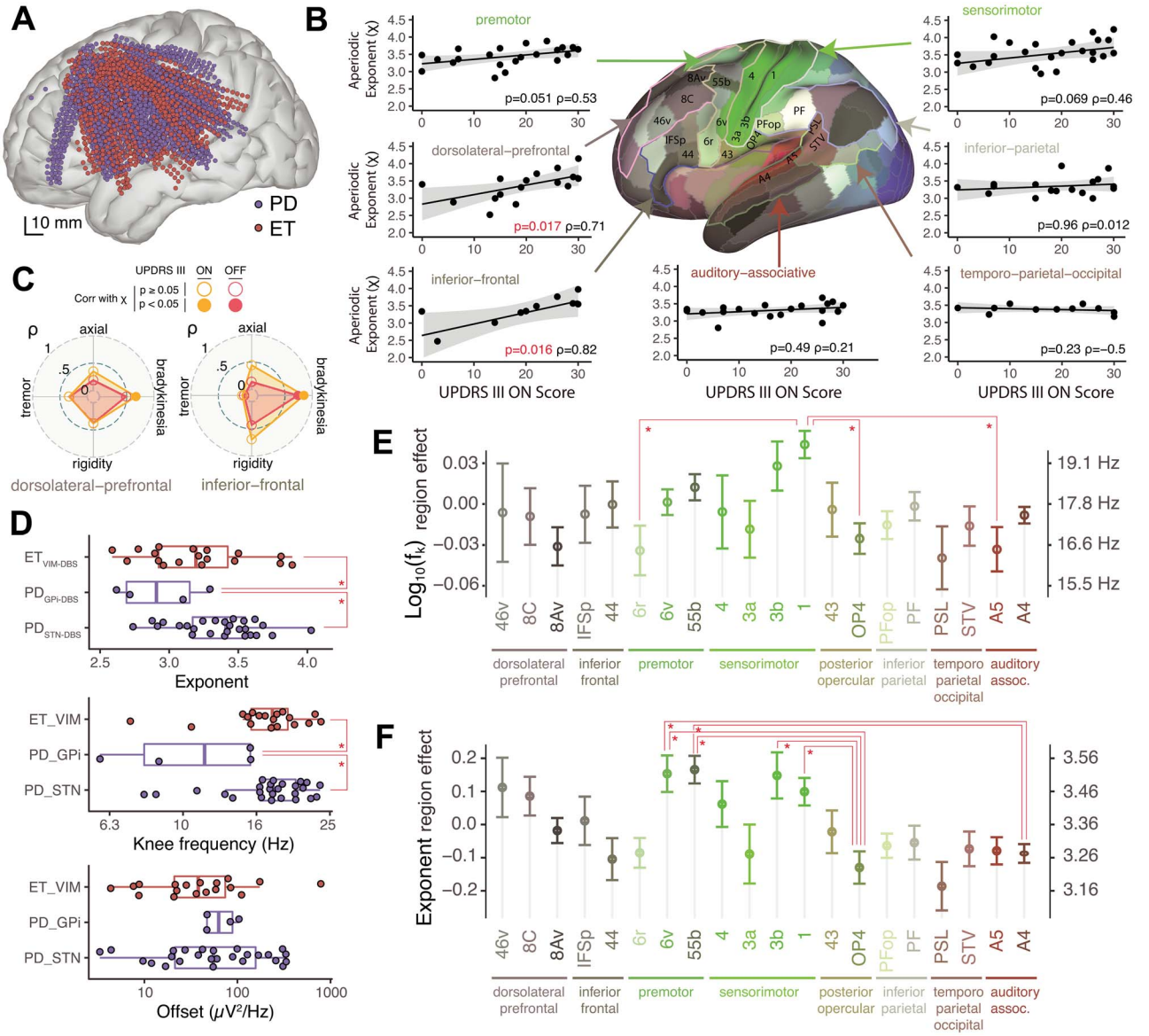

Fig. 3. Cortical aperiodic parameters correlate with PD severity and anatomical regions. (A) Anatomical localization of ECoG electrodes used to record cortical activity from the left hemisphere from Parkinson's disease (PD) and essential tremor (ET) patients undergoing DBS surgery. (B) Correlation between preoperative UPDRS-III ON score and aperiodic exponents from sampled cortical regions in PD patients undergoing STN-DBS surgery. Each point represents the median aperiodic exponent for a subject, across all available runs and ECoG contacts over a given cortical region. The shaded region represents CI_{95} of a linear fit. Spearman's ρ and FDR-corrected P-value are indicated in each panel. The central panel shows a lateral view of an inflated brain with the cortical parcellation, and regions defined by MMP1 (Glasser et al. 2016). (C) Post-hoc analysis for the dorsolateral-prefrontal and interior-frontal regions. Polar plots show Spearman's ρ correlation values between the aperiodic exponents (as shown in B) and preoperative UPDRS III ON and OFF sub-scores for bradykinesia, rigidity, tremor, and axial symptoms (Goetz et al. 2008). Significant correlations (FDR-corrected, $\alpha = 0.05$) are indicated by filled dots. (D) Distribution of cortical aperiodic exponent (top), knee frequency (center), and offset (bottom), grouped by diagnosis and subcortical DBS target (each dot represents the median across all ECoG channels and runs for a subject, and dots are jittered vertically to avoid overplotting). Boxes extend from the first to third quartile, median is indicated with a thick vertical line, and whiskers extend up to the most extreme point with 1.5 times the inter-quantile-range from the box edge (Tukey convention). Lines connecting boxes and asterisks indicate significant difference (Fisher-Pitman permutation test, $\alpha = 0.05$). E) Aperiodic knee frequency cortical-region effect (after accounting for subject effect) vs. anatomical regions, as defined in the MMP1 atlas, for regions sampled from 10 or more subjects. To avoid effects from differences in sampling density, statistics were done on the average per region per subject. Error bars indicate the SEM across subjects. Significant differences denoted by thin lines and asterisks (Tukey's HSD test, $\alpha = 0.05$). Scale on the right indicates mapping of the region-effect to knee frequencies of an "average" subject. (F) Same as (E) for the aperiodic exponent (PD: Parkinson's disease, ET: essential tremor, UPDRS: Unified Parkinson's Disease Rating Score, VIM: ventral intermediate nucleus of the thalamus, STN: subthalamic nucleus, GPi: globus pallidus internus, CI_{95}: 95% confidence interval, FDR: false discovery rate, MMP1: Multi-Modal Parcellation 1 Atlas).

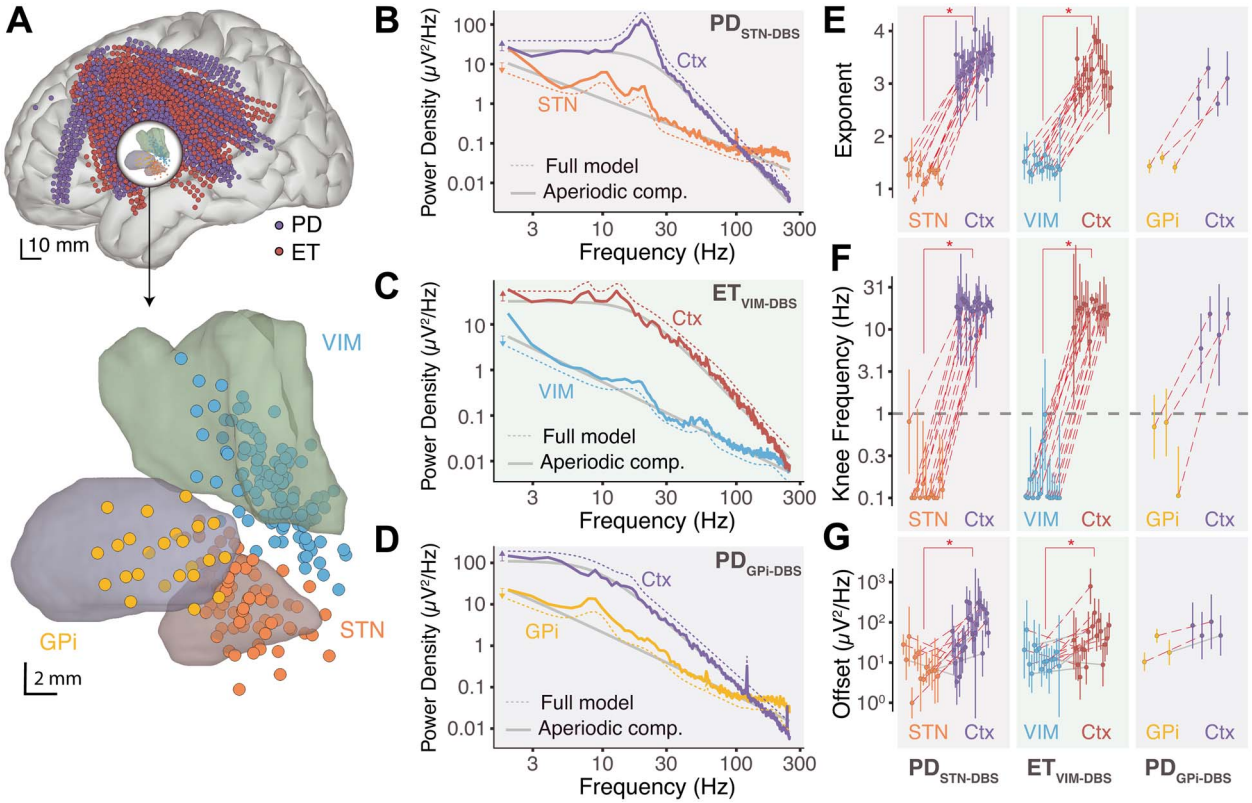

Fig. 4. Power spectra of extracellular potentials from STN, VIM, and GPi show no knee and lower aperiodic exponent than cortical recordings. (A) Anatomical localizations of cortical and subcortical electrodes from the DBS lead relative to the STN, GPi, and VIM (DISTAL and Morel atlases, respectively). (B) Representative example of power spectra, aperiodic component (continuous lines), and full model fit (dashed lines) for an STN and a cortical contact from the same subject. Note that the full-model fits were displaced vertically for visual clarity, as indicated by the arrows on the left of the plot. (C) Same as (B) for VIM. (D) Same as (B) for GPi. (E) Distribution of aperiodic exponents for STN, VIM, and GPi compared to cortex in individual subjects. Each dot corresponds to the median, and error bars to the standard deviation of all electrodes within the corresponding brain region. Dashed lines indicate significant differences between subcortical and cortical values in individual subjects (FDR-corrected permutation test, $\alpha = 0.05$). Overarching solid lines and asterisks indicate significant group-level differences (paired Wilcoxon test, $\alpha = 0.05$). (F) Same as (E) for the aperiodic knee frequency. Note that the y axis is in log-scale. The dashed horizontal gray line represents the smallest positive frequency acquired $\mathbf{f_{min}}$. Fits with knee frequencies smaller than $\mathbf{f_{min}}$ indicate spectra without observable knee. (G) Same as (E) for the aperiodic offset (PD: Parkinson's disease, ET: essential tremor, VIM: ventral intermediate nucleus of the thalamus, STN: subthalamic nucleus, GPi: globus pallidus internus, Ctx: cortex).

Table 1. Mean and dispersion of aperiodic parameters across patient cohorts and brain structures.

Cohort	Location	Electrode type	N_s	Exponent	Offset (μV^2/Hz)	f_k (Hz)	$P(f_k < f_{min})$	τ (ms)
$PD_{STN\text{-}DBS}$	STN	DBS lead	13	1.30 ± 0.21	7.6 [2.9; 20]	< 1	85 ± 4%	> 159
	Cortex	ECoG	26	3.41 ± 0.30	55 [15; 208]	17.6 [13.3; 23.3]	1.1 ± 0.2%	9.0 [6.8; 12.7]
$ET_{VIM\text{-}DBS}$	VIM	DBS lead	15	1.42 ± 0.14	11.7 [6.0; 23]	< 1	87 ± 3%	> 159
	Cortex	ECoG	18	3.20 ± 0.36	38 [11; 133]	17.0 [12.9; 22.6]	0.9 ± 0.2%	9.4 [7.0; 12.3]
$PD_{GPi\text{-}DBS}$	GPi	DBS lead	3	1.43 ± 0.10	17.8 [8.4; 38]	< 1	73 ± 9%	> 159
	Cortex	ECoG	4	2.91 ± 0.32	63 [42; 94]	11.4 [7.2; 18.2]	1.6 ± 0.6%	13.9 [8.7; 22.1]
EP_{sEEG}	Thalamus	sEEG	8	1.33 ± 0.23	4.2 [1.0; 18.2]	< 1	79 ± 4%	> 159
	Cortex	sEEG	8	2.96 ± 0.36	96 [14; 664]	7.6 [3.1; 18.3]	3.7 ± 1.6%	20.9 [8.7; 51.3]

Exponent: mean ± Standard deviation across patients. Offset (μV^2/Hz): Median [Q_{16}; Q_{84}], note the asymmetric distribution. $\mathbf{f_k}$: knee frequency in Hz, median [Q_{16}; Q_{84}]. $P(f_k < f_{min})$: percentage (± standard error) of electrodes with knee frequency lower than f_{min}. $\tau = (2\pi f_k)^{-1}$: aperiodic neural timescale in milliseconds. Abbreviations: PD, Parkinson's disease; ET, essential tremor; EP, epilepsy; STN, subthalamic nucleus; VIM, ventral intermedius nucleus of the thalamus; GPi, globus pallidus internus; N_s, number of subjects.

The calculated aperiodic knee frequency also exhibited a strikingly different distribution for STN and VIM compared to for the cortex (Table 1, $P = 2 \times 10^{-4}$ and 6×10^{-5} respectively, paired Wilcoxon test, Fig. 4F). While the cortical knee frequencies center at 17 ± 5 Hz (median ± standard deviation across subjects), those for STN, GPi, and VIM were significantly lower for all individual subjects (FDR-corrected permutation test, Fig. 4F), converging to values lower than the smallest positive frequency of the power spectra ($\mathbf{f_{min}} = 1$ Hz, gray horizontal dashed line in Fig. 4F) and, in many cases, reaching the lower boundary allowed for the fitting algorithm (0.1 Hz). It is important to note that knee frequency values smaller than $\mathbf{f_{min}}$ should not be interpreted quantitively; instead, they indicate the absence of a knee in the power spectra within the frequency range acquired. In other words, if there is a knee for the STN, GPi, and VIM power spectra, this value is lower than 1 Hz. Due to the high-pass frequency filters applied at

acquisition, exploring lower frequencies in this dataset is not possible. The proportion of power spectra without a knee $P(f_k < f_{min})$ is significantly higher for STN, VIM, and GPi recordings than for cortical recordings (Table 1, $P < 10^{-6}$, Fisher test).

The fitting range used for *specparam* can have substantial effects on the aperiodic parameters (Gerster et al. 2022). Therefore, we performed a fitting range sensitivity analysis (Fig. S6) and verified that our results are robust to the frequency ranged used. Importantly, the aperiodic parameters (including the knee) are not substantially modified by removing beta frequencies (12–30 Hz) from the fitting range (Fig. S6, rightmost panels), indicating that the prominent beta oscillations are not affecting the estimation of aperiodic parameters. We also calculated the PSD at higher frequencies for selected channels from the 30-kHz recordings, observing that the noise floor starts around 250 Hz (Fig. S7).

Given the large difference observed in aperiodic parameters for STN, GPi, and VIM as compared to cortex, we asked if these differences are specific to the types of electrodes used to record from subcortical nuclei in movement disorder patients or, on the contrary, generalize to other electrode types, subcortical structures, and diagnoses. To this end, we explored baseline recordings from 8 epilepsy patients undergoing intracranial monitoring with electrodes implanted in the thalamus to assess thalamic participation in the hypothesized seizure network and potential for therapeutic neuromodulation (Richardson 2022) (Fig. 5A). In these recordings, the same type of stereo-EEG electrode contacts, and in some cases, contacts on the same electrode, were used for cortical and thalamic targets. Thalamic contacts covered several thalamic nuclei from the ventral division (VLpd, VPLp, VLpv, VLa, VPM) to intralaminar nuclei (CM, MDpc, Pf, CL) (Morel 2007) (see Table S3), whereas selected cortical contacts covered parietal and frontal regions (Fig. 5A). As before, we found that thalamic power spectra show no observable knee, whereas cortical spectra from the same patients show prominent aperiodic knees (Fig. 5B).

A significant difference in aperiodic exponent between cortical and thalamic electrodes was observed ($P = 0.008$, paired Wilcoxon test, Fig. 5C, Table 1), consistent with the results obtained from movement disorder patients (Fig. 4E). This difference holds at the single-subject level, showing consistent changes across subjects (FDR-corrected permutation test, red dashed lines, Fig. 5C). The aperiodic knee frequency also showed significant differences for thalamic and cortical contacts (Fig. 5D), with thalamic values falling almost exclusively below $\mathbf{f_{min}}$ (smallest positive frequency of the spectra) and cortical values above this threshold ($P < 10^{-6}$, Fisher exact test). A sensitivity analysis showed that reducing the frequency range used in the fitting can result in larger values for the aperiodic knee only in thalamic sEEG recordings (Fig. S8D), which could be due to the noise-floor starting at lower frequencies (Fig. S8G). Nevertheless, the differences between thalamic and cortical knee values remained significant (Fig. S8G center).

Note that the aperiodic exponent of thalamic sEEG recordings in epilepsy patients (1.33 ± 0.23) was not significantly different than that of DBS lead recordings in movement disorder patients (Table 1, $P > 0.05$ for all pairwise comparisons by FDR-corrected permutation test). Similarly, the knee frequency extracted was below the cutoff value of $f_{min} = 1$ Hz, as for DBS recordings.

Discussion

Almost every cortical region projects to and receives projections from the thalamus and other subcortical structures (Caviness and Frost 1980; Sherman 2016). These interactions provide a substrate for communication between distant cortical regions, facilitating spatial integration of the brain (Grant et al. 2012) and creating circuits with massive convergence and divergence in cell number at different nodes, as in the cortico-basal ganglia-thalamo-cortical loop (Wilson 2013; Bergman 2021). This organization involves regions whose cell types differ on many levels, including channel and receptor expression, morphology, cytoarchitectures, and proportions of excitatory and inhibitory interactions. These differences allow for distinct dynamical behaviors and computational properties across brain structures.

In this study, we systematically analyzed the aperiodic component of brain recordings from multiple locations of the cortico-basal ganglia-thalamo-cortical loop by fitting a phenomenological model to the power spectra of LFPs (Donoghue et al. 2020). We developed a novel parameterization of the aperiodic component with the following advantages: (1) well-defined units for all parameters, (2) easily interpretable parameters, (3) structurally uncorrelated parameters, (4) parameters with more constrained physiological ranges, and (5) the ability to fit spectra with or without an aperiodic "knee" using the same model (see Fig. 2 and Supplementary Materials). Interestingly, even with the novel parameterization of the aperiodic exponent, which removes structural correlations between parameters (Cedersund and Roll 2009), a residual positive correlation between the aperiodic knee and the exponent of the spectra (Fig. S2B) was observed, suggesting that these parameters could be coupled.

Using this model to fit power spectra from baseline ECoG recordings from patients undergoing DBS implantation surgery (inter-trial-gaps of a speech task as described in methods), we found that dorsolateral-prefrontal and inferior-frontal cortical aperiodic exponents correlate with Parkinson's disease severity as assessed by the preoperative UPDRS III (ON-medication, Fig. 3B). This novel result aligns with an MEG finding showing higher aperiodic exponents for PD patients compared to healthy controls (Vinding et al. 2020). In our data, the correlation with the aperiodic exponent did not reach significance for the preoperative UPDRS-OFF score, even though patients were in an OFF state during the intra-operative recordings. This could be due to less sensitivity or higher variability for the UPDRS-OFF score (compared to the ON score) for the clinical population undergoing DBS treatment, which is biased to high symptom severity. There were no significant correlations of the STN LFP aperiodic exponent with UPDRS-III score (ON nor OFF levodopa), consistent with a recent report in humans (Wiest et al. 2022), but opposite to findings in rats (Kim et al. 2022).

Total beta power correlates with PD disease severity in the basal ganglia (Brown et al. 2001; Cassidy et al. 2002; Kühn et al. 2004) and sensory-motor cortex (Williams et al. 2002; Pollok et al. 2012). *Specparam* was designed to decouple oscillations from the underlying aperiodic component, which reflects features of the entire spectrum, not just a specific band. Indeed, accounting for the aperiodic component reveals a stronger correlation between beta oscillations and Parkinsonian symptoms (Martin et al. 2018; Kim et al. 2022). However, estimations of aperiodic parameters can be affected by oscillatory components that extend beyond the fitting range (Gerster et al. 2022). This is not the case for our data since beta (12–30 Hz) frequencies are above the lower frequency acquired ($f_{min} = 1$ Hz), and removing beta frequencies does not substantially affect the aperiodic parameters (Supplementary Fig. S6). Additionally, we included a regularization term penalizing peaks below f_{min} to avoid this pitfall (see Methods and Fig. S8I). Indeed, the fact that we obtained a significant correlation of the aperiodic exponent with UPDRS for frontal cortex but not in the

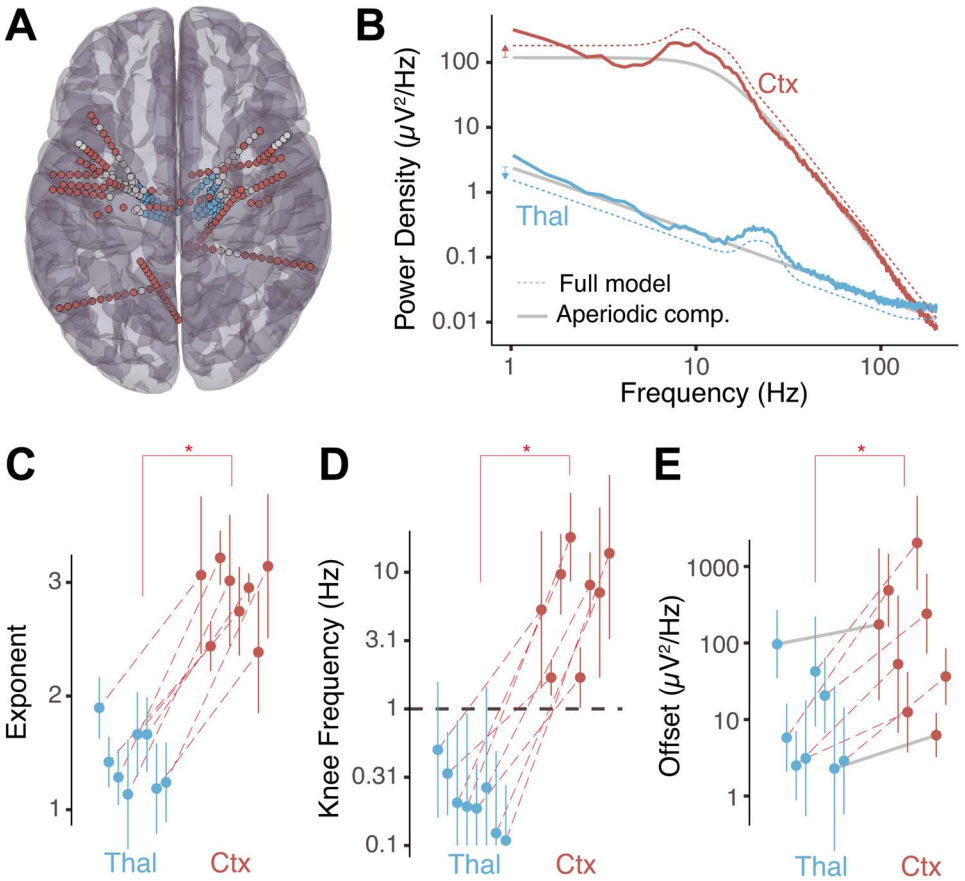

Fig. 5. Power spectra from thalamic sEEG recordings show no knee and lower aperiodic exponent than cortical sEEG signals. (A) Anatomical localizations of selected sEEG electrodes for epilepsy patients with thalamic implantations. (B) Representative example of power spectra aperiodic component (continuous line) and full-model fit (dashed lines) from a cortical sEEG contact (Ctx) and thalamic sEEG (Thal) recordings. The full-model fits were displaced vertically for visual clarity, as indicated by the colored arrows on the left. (C) Distribution of aperiodic exponents for thalamic recordings compared to cortex in individual subjects. Each dot corresponds to the median, and the error bars to the standard deviation of all contacts within the thalamus and cortex. Dashed lines indicate significant difference in values between thalamus and cortex in individual subjects (FDR-corrected permutation test, $\alpha = 0.05$). Overarching solid lines and asterisks indicate significant group-level differences (paired Wilcoxon test, $\alpha = 0.05$). (D) Same as (C) for the knee frequency. Note that the y axis is in log-scale. The dashed horizontal line represents $\mathbf{f}_{\mathbf{min}}$. (E) Same as (C) for the aperiodic offset. (Ctx: cortex, Thal: thalamus).

basal ganglia (which has prominent pathological beta oscillations) suggests that the method is correctly decoupling the aperiodic component from oscillatory features.

The main finding of this work is the conspicuous difference in the aperiodic component of the spectra between cortical recordings and those of basal ganglia and thalamic nuclei (Figs. 4 and 5). Whereas cortical recordings showed an aperiodic knee with significant changes across cortical regions (Fig. 3E, consistent with recent reports; Muthukumaraswamy and Liley 2018; Gao et al. 2020; Chaoul and Siegel 2021), spectra from basal ganglia and thalamic nuclei show no knee, an observation we could systematically evaluate thanks to the novel parameterization of the aperiodic component. Spectra from subcortical regions showed an aperiodic exponent close to one ($\chi = 1.3 \pm 0.2$), significantly smaller than in cortex ($\chi = 3.2 \pm 0.3$). These results are reproducible across patients, two medical centers, electrode types, recording systems, diagnoses, and subcortical structures. Furthermore, the value for the aperiodic exponent in the STN we measured is consistent with recent studies that estimated this parameter (Huang et al. 2020; Wiest et al. 2022).

A limitation of this work is that for the PD and ET cohorts, the ECoG electrodes lie over the pia mater, whereas the DBS leads penetrate the brain parenchyma. However, our data from epilepsy patients were recorded from the same type of sEEG electrodes for cortical and thalamic regions. Notably, these multi-contact electrodes are similar in size, shape, and impedance value to DBS lead contacts (Supplementary Table S1). We observed the same qualitative difference in aperiodic parameters between cortical and subcortical regions in both datasets, suggesting that these differences cannot be fully explained by electrode type and are due to structural and/or functional properties of the recorded brain areas. Another important limitation of our work is that different subcortical regions were recorded from different clinical populations. Due to this unavoidable confound, we did not compare parameters across subcortical regions and instead limited our analysis of cortical vs. subcortical aperiodic activity to within-subject comparisons. Another limitation of the model is the assumption of constant power for frequencies below the knee. Fitting an additional aperiodic exponent could potentially improve the fits at frequencies below the knee. However, we did not implement this modification since it would increase the complexity of the model and could exacerbate parameter unidentifiability.

Neural morphology affects the shape and amplitude of extracellular potentials and could explain the differences in aperiodic activity observed between cortical and subcortical structures. For example, cells with large spatial separation between current

sinks and return currents (like cortical pyramidal neurons) induce substantial extracellular ionic flows and large perturbations of the extracellular potential (Johnston and Wu 1995). In contrast, neurons with roughly spherically symmetric dendritic arbors (like thalamocortical or STN neurons) do not produce strong current dipoles, with smaller contributions to recorded extracellular field potentials (Johnston and Wu 1995; Buzsáki et al. 2012). However, synaptic inputs to subcortical structures may have asymmetric distributions which can produce measurable field potentials (Lindén et al. 2010; Buzsáki et al. 2012; Tanaka and Nakamura 2019), for example, having inhibitory synapses closer to the soma and more distal excitatory inputs (Wilson 2010; Lempka and McIntyre 2013; Mazzoni et al. 2015).

Although neuronal densities are comparable between cortical gray matter, STN, and VIM (Lévesque and Parent 2005; Bergman 2021), the spatial arrangement of neurons can also have a large effect on the recorded extracellular potential (Johnston and Wu 1995; Gold et al. 2006; Pettersen et al. 2008). In neuronal populations organized in layers, such as the six-layered neocortex, simultaneous contributions from multiple similarly oriented cells will add up to give large fluctuations of the extracellular potential. In contrast, in neurons with spatially isotropic arrangements, as in subcortical nuclei, simultaneous contributions from different units in diverse orientations can cancel out to some extent, producing smaller extracellular potentials (Johnston and Wu 1995). These structural differences can explain why the overall power of field potentials is lower in subcortical nuclei than in neocortex. However, they do not explain why the aperiodic exponent and knee differ across these structures.

Several mechanisms have been suggested as the origin of the $1/f^{\chi}$ aperiodic component, including ionic diffusion and induction of electric fields in passive cells (Bédard et al. 2006a; Bédard and Destexhe 2009). The shape and length of the dendrites and the location of the synaptic input can give rise to different frequency dependences of the intrinsic dendritic filtering (Lindén et al. 2010). The distinct morphology of cortical versus thalamic and basal ganglia neurons could contribute to the observed difference in aperiodic exponent. However, this parameter depends on dynamical aspects of neural activity and cannot be fully explained by morphology and cytoarchitecture with studies showing the change in aperiodic exponent in the STN with Propofol anesthesia (Huang et al. 2020), dopaminergic medication, and DBS treatment (Wiest et al. 2022).

The origins of the aperiodic exponent have also been linked to functional differences such as post-synaptic currents' profile and characteristic duration. For example, sharp rise and exponential decays for post-synaptic currents give rise to a $1/f^2$ decline of power (Bédard et al. 2006b; Miller et al. 2009; Milstein et al. 2009). Transitions between UP and DOWN states (i.e. rapid trains of correlated synaptic inputs followed by quiescent periods) can also give rise to power spectra following $1/f^2$ decline (Milstein et al. 2009; Baranauskas et al. 2012). Different types of stochastic noise can affect the aperiodic exponent (Kramer and Chu 2023), whereas Poissonian inputs that are uncorrelated across cells do not contribute to the frequency dependency of the spectra (Bédard et al. 2006b; Miller et al. 2009; Milstein et al. 2009). Interestingly, there is a surprisingly low spike-timing correlation in the pallidum (Nini et al. 1995; Raz et al. 2000; Bar-Gad et al. 2003) and structures with strong pallidal input, including GPi, STN, and several nuclei of the ventral thalamus will have low input correlation, which contributes to the low amplitude (Lindén et al. 2011) and slow decline with frequency of the power spectra in these regions. Finally, the ratio of excitatory to inhibitory inputs can also affect the aperiodic exponent of the spectra (Gao et al. 2017; Wiest et al. 2023). Since multiple functional characteristics can affect the aperiodic exponent, it is not possible to directly ascribe a change in χ to a single phenomenon (i.e. changes in E/I balance) without additional experiments or analysis, especially when comparing across brain structures.

There is no consensus on the physiological interpretation of the aperiodic knee and its change across brain structures. Miller et al. showed in ECoG recordings an aperiodic slope of $\chi = 2$ for frequencies above 15 Hz up to a "knee" around 75 Hz, at which the aperiodic slope changed to $\chi = 4$, implying the existence of a characteristic timescale $\tau = (2\pi f_k)^{-1} = 2-4\ ms$ (Miller et al. 2009). Using similar reasoning on the knee observed around 10 Hz, Gao et al. proposed the existence of an "aperiodic neural timescale" (of around 10–50 ms) that can be interpreted as the characteristic duration of an aperiodic fluctuation of the LFP (Gao et al. 2020). This timescale is approximated from the power spectra's aperiodic knee, via the Wiener–Khinchin theorem that relates the PSD function and the autocorrelation function (Gao et al. 2020). In our data, this timescale is in the range of 10–20 ms (Table 1) and changes across cortical locations (Fig. 3e), which is consistent with previous findings and suggests that this parameter might be reflecting an intrinsic feature of cortical micro-circuitry and computation (Gao et al. 2020).

The lack of an observable aperiodic knee for thalamic and basal ganglia recordings (i.e. the fitted value is lower than the cutoff frequency f_{min}; Figs 4 and 5) could be interpreted as reflecting the absence of any characteristic duration of aperiodic fluctuations (strict $1/f$ power law). However, these regions' neural morphology and cytoarchitecture might prevent characteristic aperiodic fluctuations from being reflected in LFPs. Alternatively, the aperiodic neural timescale could be longer than what can be detected by our method due to the technical limitations of the recording system, which result in a lower bound of 159 ms ($\tau > (2\pi\ f_{\text{min}})^{-1} = 159\ \textbf{ms}$ for $f_{\text{min}} = 1\ \textbf{Hz}$) for the subcortical LFPs. This interpretation suggests that basal ganglia and ventral thalamic nuclei are slower than cortex in terms of their aperiodic fluctuations. Although speculative, this interpretation suggests that the basal ganglia-thalamo-cortical loop could be a site of temporal integration, a notion that aligns well with the known role of this circuit in spatial integration, action selection, and motor control (Mink 1996; DeLong and Wichmann 2010; Turner and Desmurget 2010; Grant et al. 2012; Bergman 2021).

Acknowledgments

We thank our patient-participants for their time and effort.

Author contributions

Alan Bush (Conceptualization, Data curation, Formal analysis, Investigation, Software, Supervision, Writing—original draft, Writing—review & editing), Jasmine Zou (Data curation, Formal analysis, Investigation, Software), Witold Lipski (Data curation, Investigation), Vasileios Kokkinos (Data curation), Robert Richardson (Conceptualization, Investigation, Project administration, Supervision, Writing—review & editing). WJL and RMR performed the intraoperative recordings. AB, WJL, and VK reconstructed the electrode localizations. AB, WJL, VK, and JZ preprocessed electrophysiological data. AB and JZ developed and implemented the model and analyzed data. AB and RMR conceived the study and wrote the manuscript. All authors discussed the results and commented on the manuscript.

Supplementary material

Supplementary material is available at *Cerebral Cortex* online.

Funding

This work was funded by the National Institute of Health (U01NS098969 and U01NS117836 to R.M.R.).

Conflict of interest statement: None declared.

Data availability

The data of this study is hosted in the Data Archive BRAIN Initiative (DABI, https://dabi.loni.usc.edu/dsi/1U01NS098969) and is available upon request.

References

Avants BB, Epstein CL, Grossman M, Gee JC. Symmetric diffeomorphic image registration with cross-correlation: evaluating automated labeling of elderly and neurodegenerative brain. *Med Image Anal*. 2008:12:26–41.

Baranauskas G, Maggiolini E, Vato A, Angotzi G, Bonfanti A, Zambra G, Spinelli A, Fadiga L. Origins of 1/f 2 scaling in the power spectrum of intracortical local field potential. *J Neurophysiol*. 2012:107(3):984–994. https://doi.org/10.1152/jn.00470.2011.

Bar-Gad I, Heimer G, Ritov Y, Bergman H. Functional correlations between neighboring neurons in the primate globus pallidus are weak or nonexistent. *J Neurosci*. 2003:23(10):4012–4016. https://doi.org/10.1523/JNEUROSCI.23-10-04012.2003.

Basar E, Güntekin B. Review of delta, theta, alpha, beta and gamma response oscillation in neuropsychiatric disorders. In: Basar E, Basar-Eroglu C, Ozerdem A, Rossini PM, Yener GG, editors. *Application of brain oscillations in neuropsychiatric diseases, Supplements to clinical neurophysiology*. Elsevier Science Health Science, Vol. 62, 2013. pp. 303–341.

Bédard C, Destexhe A. Macroscopic models of local field potentials and the apparent 1/f noise in brain activity. *Biophys J*. 2009:96(7):2589–2603. https://doi.org/10.1016/j.bpj.2008.12.3951.

Bédard C, Kröger H, Destexhe A. Model of low-pass filtering of local field potentials in brain tissue. *Phys Rev E*. 2006a:73(5):051911. https://doi.org/10.1103/PhysRevE.73.051911.

Bédard C, Kröger H, Destexhe A. Does the 1/f frequency scaling of brain signals reflect self-organized critical states? *Phys Rev Lett*. 2006b:97(11):118102. https://doi.org/10.1103/PhysRevLett.97.118102.

Berger H. Über das Elektrenkephalogramm des Menschen. *Archiv Psychiatr Nervenkr*. 1929:87(1):527–570. https://doi.org/10.1007/BF01797193.

Bergman H. *The hidden life of the basal ganglia*. Cambridge, MA: MIT Press; 2021.

Bretz F, Hothorn T, Westfall P (2011) *Multiple comparisons using R*. Boca Raton, Florida: CRC Press 1. https://doi.org/10.7551/mitpress/14075.001.0001.

Brown P, Oliviero A, Mazzone P, Insola A, Tonali P, Lazzaro VD. Dopamine dependency of oscillations between subthalamic nucleus and pallidum in Parkinson's disease. *J Neurosci*. 2001:21:1033–1038.

Bush A, Chrabaszcz A, Peterson V, Saravanan V, Dastolfo-Hromack C, Lipski WJ, Richardson RM. Differentiation of speech-induced artifacts from physiological high gamma activity in intracranial recordings. *NeuroImage*. 2022:250:118962. https://doi.org/10.1016/j.neuroimage.2022.118962.

Buzsáki G, Anastassiou CA, Koch C. The origin of extracellular fields and currents — EEG, ECoG, LFP and spikes. *Nat Rev Neurosci*. 2012:13(6):407–420. https://doi.org/10.1038/nrn3241.

Cassidy M, Mazzone P, Oliviero A, Insola A, Tonali P, Lazzaro VD, Brown P. Movement-related changes in synchronization in the human basal ganglia. *Brain*. 2002:125(6):1235–1246. https://doi.org/10.1093/brain/awf135.

Caviness VS, Frost DO. Tangential organization of thalamic projections to the neocortex in the mouse. *J Comp Neurol*. 1980:194(2):335–367. https://doi.org/10.1002/cne.901940205.

Cedersund G, Roll J. Systems biology: model based evaluation and comparison of potential explanations for given biological data. *FEBS J*. 2009:276(4):903–922. https://doi.org/10.1111/j.1742-4658.2008.06845.x.

Chaoul AI, Siegel M. Cortical correlation structure of aperiodic neuronal population activity. *NeuroImage*. 2021:245:118672.

Colombo MA, Napolitani M, Boly M, Gosseries O, Casarotto S, Rosanova M, Brichant J-F, Boveroux P, Rex S, Laureys S, et al. The spectral exponent of the resting EEG indexes the presence of consciousness during unresponsiveness induced by propofol, xenon, and ketamine. *NeuroImage*. 2019:189:631–644. https://doi.org/10.1016/j.neuroimage.2019.01.024.

Dave S, Brothers TA, Swaab TY. 1/f neural noise and electrophysiological indices of contextual prediction in aging. *Brain Res*. 2018:1691:34–43. https://doi.org/10.1016/j.brainres.2018.04.007.

DeLong M, Wichmann T. Changing views of basal ganglia circuits and circuit disorders. *Clin Eeg Neurosci*. 2010:41(2):61–67. https://doi.org/10.1177/155005941004100204.

Donoghue T, Haller M, Peterson EJ, Varma P, Sebastian P, Gao R, Noto T, Lara AH, Wallis JD, Knight RT, et al. Parameterizing neural power spectra into periodic and aperiodic components. *Nat Neurosci*. 2020:23(12):1655–1665. https://doi.org/10.1038/s41593-020-00744-x.

Engel AK, Fries P, Singer W. Dynamic predictions: oscillations and synchrony in top–down processing. *Nat Rev Neurosci*. 2001:2(10):704–716. https://doi.org/10.1038/35094565.

Ewert S, Plettig P, Li N, Chakravarty MM, Collins DL, Herrington TM, Kühn AA, Horn A. Toward defining deep brain stimulation targets in MNI space: a subcortical atlas based on multimodal MRI, histology and structural connectivity. *NeuroImage*. 2018:170:271–282. https://doi.org/10.1016/j.neuroimage.2017.05.015.

Fischl B, Salat DH, Busa E, Albert M, Dieterich M, Haselgrove C, van der Kouwe A, Killiany R, Kennedy D, Klaveness S, et al. Whole brain segmentation automated labeling of neuroanatomical structures in the human brain. *Neuron*. 2002:33(3):341–355. https://doi.org/10.1016/S0896-6273(02)00569-X.

Fonov V, Evans AC, Botteron K, Almli CR, RC MK, Collins DL, Group the BDC. Unbiased average age-appropriate atlases for pediatric studies. *NeuroImage*. 2011:54:313–327.

Gao R, Peterson EJ, Voytek B. Inferring synaptic excitation/inhibition balance from field potentials. *NeuroImage*. 2017:158:70–78. https://doi.org/10.1016/j.neuroimage.2017.06.078.

Gao R, van den Brink RL, Pfeffer T, Voytek B. Neuronal timescales are functionally dynamic and shaped by cortical microarchitecture. *elife*. 2020:9:e61277. https://doi.org/10.7554/eLife.61277.

Gerster M, Waterstraat G, Litvak V, Lehnertz K, Schnitzler A, Florin E, Curio G, Nikulin V. Separating neural oscillations from aperiodic 1/f activity: challenges and recommendations. *Neuroinformatics*. 2022:20(4):991–1012. https://doi.org/10.1007/s12021-022-09581-8.

Glasser MF, Coalson TS, Robinson EC, Hacker CD, Harwell J, Yacoub E, Ugurbil K, Andersson J, Beckmann CF, Jenkinson M, et al. A multimodal parcellation of human cerebral cortex. *Nature*. 2016:536:171–178.

Goetz CG, Tilley BC, Shaftman SR, Stebbins GT, Fahn S, Martinez–Martin P, Poewe W, Sampaio C, Stern MB, Dodel R, et al. Movement Disorder Society-sponsored revision of the Unified Parkinson's Disease Rating Scale (MDS-UPDRS): scale presentation and clinimetric testing results. *Mov Disord*. 2008:23(15):2129–2170. https://doi.org/10.1002/mds.22340.

Gold C, Henze DA, Koch C, Buzsáki G. On the origin of the extracellular action potential waveform: a modeling study. *J Neurophysiol*. 2006:95(5):3113–3128. https://doi.org/10.1152/jn.00979.2005.

Grant E, Hoerder-Suabedissen A, Molnár Z. Development of the corticothalamic projections. *Front Neurosci*. 2012:6:53. https://doi.org/10.3389/fnins.2012.00053.

Horn A, Li N, Dembek TA, Kappel A, Boulay C, Ewert S, Tietze A, Husch A, Perera T, Neumann WJ, et al. Lead-DBS v2: towards a comprehensive pipeline for deep brain stimulation imaging. *NeuroImage*. 2019:184:293–316. https://doi.org/10.1016/j.neuroimage.2018.08.068.

Hothorn T, Hornik K, van de Wiel MA, Zeileis A. Implementing a class of permutation tests: the coin package. *Wiley Interdiscip Rev Comput Statistics*. 2008:1:128–129. https://doi.org/10.1016/j.neuroimage.2018.08.068.

Huang Y, Hu K, Green AL, Ma X, Gillies MJ, Wang S, Fitzgerald JJ, Pan Y, Martin S, Huang P, et al. Dynamic changes in rhythmic and arrhythmic neural signatures in the subthalamic nucleus induced by anaesthesia and tracheal intubation. *Br J Anaesth*. 2020:125(1):67–76. https://doi.org/10.1016/j.bja.2020.03.014.

Johnston D, Wu SM-S. *Foundations of cellular neurophysiology*. Cambridge, Massachusetts: The MIT Press; 1995.

Jost ST, Strobel L, Rizos A, Loehrer PA, Ashkan K, Evans J, Rosenkranz F, Barbe MT, Fink GR, Franklin J, et al. Gender gap in deep brain stimulation for Parkinson's disease. *NPJ Parkinsons Dis*. 2022:8(1):47.

Kim J, Lee J, Kim E, Choi JH, Rah J-C, Choi J-W. Dopamine depletion can be predicted by the aperiodic component of subthalamic local field potentials. *Neurobiol Dis*. 2022:168:105692. https://doi.org/10.1016/j.nbd.2022.105692.

Kramer MA, Chu CJ. The 1/f-like behavior of neural field spectra are a natural consequence of noise driven brain dynamics. *bioRxiv*. 2023. https://doi.org/10.1101/2023.03.10.532077.

Kühn AA, Williams D, Kupsch A, Limousin P, Hariz M, Schneider G, Yarrow K, Brown P. Event-related beta desynchronization in human subthalamic nucleus correlates with motor performance. *Brain*. 2004:127(4):735–746. https://doi.org/10.1093/brain/awh106.

Kuznetsova A, Brockhoff PB, Christensen RHB. lmerTest package: tests in linear mixed effects models. *J Stat Softw*. 2017:82(13). https://doi.org/10.18637/jss.v082.i13.

Lempka SF, McIntyre CC. Theoretical analysis of the local field potential in deep brain stimulation applications. *PLoS One*. 2013:8(3):e59839.

Lendner JD, Helfrich RF, Mander BA, Romundstad L, Lin JJ, Walker MP, Larsson PG, Knight RT. An electrophysiological marker of arousal level in humans. *elife*. 2020:9:e55092. https://doi.org/10.7554/eLife.55092.

Lévesque J, Parent A. GABAergic interneurons in human subthalamic nucleus. *Movement Disord*. 2005:20:574–584. https://doi.org/10.1002/mds.20374.

Lindén H, Pettersen KH, Einevoll GT. Intrinsic dendritic filtering gives low-pass power spectra of local field potentials. *J Comput Neurosci*. 2010:29:423–444. https://doi.org/10.1007/s10827-010-0245-4.

Lindén H, Tetzlaff T, Potjans TC, Pettersen KH, Grün S, Diesmann M, Einevoll GT. Modeling the spatial reach of the LFP. *Neuron*. 2011:72(5):859–872. https://doi.org/10.1016/j.neuron.2011.11.006.

Martin S, Iturrate I, Chavarriaga R, Leeb R, Sobolewski A, Li AM, Zaldivar J, Peciu-Florianu I, Pralong E, Castro-Jiménez M, et al. Differential contributions of subthalamic beta rhythms and 1/f broadband activity to motor symptoms in Parkinson's disease. *NPJ Parkinson Dis*. 2018:4:32.

Mazzoni A, Lindén H, Cuntz H, Lansner A, Panzeri S, Einevoll GT. Computing the local field potential (LFP) from integrate-and-fire network models. *PLoS Comput Biol*. 2015:11(12):e1004584. https://doi.org/10.1371/journal.pcbi.1004584.

Miller KJ, Sorensen LB, Ojemann JG, den Nijs M. Power-law scaling in the brain surface electric potential. *PLoS Comput Biol*. 2009:5(12):e1000609. https://doi.org/10.1371/journal.pcbi.1000609.

Milstein J, Mormann F, Fried I, Koch C. Neuronal shot noise and Brownian 1/f2 behavior in the local field potential. *PLoS One*. 2009:4(2):e4338. https://doi.org/10.1371/journal.pone.0004338.

Mink JW. The basal ganglia: focused selection and inhibition of competing motor programs. *Prog Neurobiol*. 1996:50(4):381–425. https://doi.org/10.1016/S0301-0082(96)00042-1.

Miskovic V, MacDonald KJ, Rhodes LJ, Cote KA. Changes in EEG multiscale entropy and power-law frequency scaling during the human sleep cycle. *Hum Brain Mapp*. 2019:40(2):538–551. https://doi.org/10.1002/hbm.24393.

Morel A. *Stereotactic atlas of the human thalamus and basal ganglia*. New York, NY: Informa Healthcare; 2007.

Muthukumaraswamy SD, Liley DTJ. 1/f electrophysiological spectra in resting and drug-induced states can be explained by the dynamics of multiple oscillatory relaxation processes. *NeuroImage*. 2018:179:582–595. https://doi.org/10.1016/j.neuroimage.2018.06.068.

Nini A, Feingold A, Slovin H, Bergman H. Neurons in the globus pallidus do not show correlated activity in the normal monkey, but phase-locked oscillations appear in the MPTP model of parkinsonism. *J Neurophysiol*. 1995:74(4):1800–1805. https://doi.org/10.1152/jn.1995.74.4.1800.

Nunez PL, Srinivasan R (2006) *Electric fields of the brain*. New York, NY: Oxford University Press. https://doi.org/10.1093/acprof:oso/9780195050387.001.0001.

Oostenveld R, Fries P, Maris E, Schoffelen J-M. FieldTrip: open source software for advanced analysis of MEG, EEG, and invasive electrophysiological data. *Comput Intell Neurosci*. 2011:2011:1–9. https://doi.org/10.1155/2011/156869.

Pettersen KH, Hagen E, Einevoll GT. Estimation of population firing rates and current source densities from laminar electrode recordings. *J Comput Neurosci*. 2008:24(3):291–313. https://doi.org/10.1007/s10827-007-0056-4.

Pollok B, Krause V, Martsch W, Wach C, Schnitzler A, Südmeyer M. Motor-cortical oscillations in early stages of Parkinson's disease. *J Physiol*. 2012:590(13):3203–3212. https://doi.org/10.1113/jphysiol.2012.231316.

Randazzo MJ, Kondylis ED, Alhourani A, Wozny TA, Lipski WJ, Crammond DJ, Richardson RM. Three-dimensional localization of cortical electrodes in deep brain stimulation surgery from intraoperative fluoroscopy. *NeuroImage*. 2016:125:515–521. https://doi.org/10.1016/j.neuroimage.2015.10.076.

Raz A, Vaadia E, Bergman H. Firing patterns and correlations of spontaneous discharge of pallidal neurons in the normal and the tremulous 1-methyl-4-phenyl-1,2,3,6-tetrahydropyridine vervet model of parkinsonism. *J Neurosci*. 2000:20:8559–8571. https://doi.org/10.1523/JNEUROSCI.20-22-08559.2000.

Richardson RM. Closed-loop brain stimulation and paradigm shifts in epilepsy surgery. *Neurol Clin*. 2022:40:355–373. https://doi.org/10.1016/j.ncl.2021.12.002.

Sherman SM. Thalamus plays a central role in ongoing cortical functioning. *Nat Neurosci*. 2016:19:533–541. https://doi.org/10.1038/nn.4269.

Tadel F, Baillet S, Mosher JC, Pantazis D, Leahy RM. Brainstorm: a user-friendly application for MEG/EEG analysis. *Comput Intell Neurosci*. 2011:2011:879716, 1–879713. https://doi.org/10.1155/2011/879716.

Tanaka T, Nakamura KC. Focal inputs are a potential origin of local field potential (LFP) in the brain regions without laminar structure. *PLoS One*. 2019:14(12):e0226028. https://doi.org/10.1371/journal.pone.0226028.

Turner RS, Desmurget M. Basal ganglia contributions to motor control: a vigorous tutor. *Curr Opin Neurobiol*. 2010:20(6):704–716. https://doi.org/10.1016/j.conb.2010.08.022.

Vinding MC, Tsitsi P, Waldthaler J, Oostenveld R, Ingvar M, Svenningsson P, Lundqvist D. Reduction of spontaneous cortical beta bursts in Parkinson's disease is linked to symptom severity. *Brain Commun*. 2020:2(1):fcaa052. https://doi.org/10.1093/braincomms/fcaa052.

Vissani M, Bush A, Lipski WJ, Fischer P, Neudorfer C, Holt LL, Fiez JA, Turner RS, Richardson RM. Speech induces spatiotemporal and frequency specific subthalamic-cortical spike-phase coupling events. *bioRxiv*. 2023. https://doi.org/10.1101/2023.10.18.562969.

Voytek B, Kramer MA, Case J, Lepage KQ, Tempesta ZR, Knight RT, Gazzaley A. Age-related changes in 1/f neural electrophysiological noise. *J Neurosci*. 2015:35(38):13257–13265. https://doi.org/10.1523/JNEUROSCI.2332-14.2015.

Welch PD. The use of fast Fourier transform for the estimation of power spectra: a method based on time averaging overt short, modified periodigrams. *IEEE Trans Audio Electroacoust*. 1967:AU-15:70–73.

Wen H, Liu Z. Separating fractal and oscillatory components in the power Spectrum of neurophysiological signal. *Brain Topogr*. 2016:29(1):13–26. https://doi.org/10.1007/s10548-015-0448-0.

Wiest C, Torrecillos F, Pogosyan A, Bange M, Muthuraman M, Groppa S, Hulse N, Hasegawa H, Ashkan K, Baig F, et al. The aperiodic exponent of subthalamic field potentials reflects excitation/inhibition balance in Parkinsonism: a cross-species study in vivo. *Biorxiv*. 2022:2022(1):23.504923. https://doi.org/10.1007/s10548-015-0448-0.

Wiest C, Torrecillos F, Pogosyan A, Bange M, Muthuraman M, Groppa S, Hulse N, Hasegawa H, Ashkan K, Baig F, et al. The aperiodic exponent of subthalamic field potentials reflects excitation/inhibition balance in Parkinsonism. *elife*. 2023:12:e82467. https://doi.org/10.7554/eLife.82467.

Williams D, Tijssen M, van Bruggen G, Bosch A, Insola A, Lazzaro VD, Mazzone P, Oliviero A, Quartarone A, Speelman H, et al. Dopamine-dependent changes in the functional connectivity between basal ganglia and cerebral cortex in humans. *Brain*. 2002:125:1558–1569.

Willis AW, Schootman M, Kung N, Wang XY, Perlmutter JS, Racette BA. Disparities in deep brain stimulation surgery among insured elders with Parkinson disease. *Neurology*. 2014:83:1684–1685.

Wilson CJ. Subthalamo-pallidal circuit. In: Shepherd GM, Grillner S, editors. *Handbook of brain microcircuits*. Oxford University Press; 2010. pp. 127–134.

Wilson CJ. Active decorrelation in the basal ganglia. *Neuroscience*. 2013:250:467–482. https://doi.org/10.1016/j.neuroscience.2013.07.032.